Global Journal of Engineering and Technology Advances
eISSN: 2582-5003
Cross Ref DOI: 10.30574/gjeta
Journal homepage: https://gjeta.com/

(RESEARCH ARTICLE)

Check for updates

Design modification of elliptical vessel solar receiver by response surface methodology

Aka CC *, Onah TO and Egwuagu OM

Department of Mechanical and Production Engineering, Enugu State University of Science and Technology Enugu, Enugu, Nigeria.

Global Journal of Engineering and Technology Advances, 2024, 19(01), 129–142

Publication history: Received on 01 March 2024; revised on 10 April 2024; accepted on 13 April 2024

Article DOI: https://doi.org/10.30574/gjeta.2024.19.1.0064

Abstract

Design modification of elliptical vessel solar receiver system by response surface methodology has been carried out. The materials used in this study were locally sourced from Kenyeta Market Enugu, Onitsha Bridge Head Market, and Idumota Market Lagos. These materials were sourced based on categories of components element: support mechanisms made of mild steel plates, bolts, nuts, clamps, and water as heat transfer fluid. The reflector is made of aluminum foil tape while the vessel has a glass cover fitted with bolts and nuts, the receiver is made of copper pipe, aluminum pipe, galvanized iron pipes, and stainless steel pipes. The pipes were fitted into the vessel with chlorinated polyvinyl chloride 3/4 joint pipes, and journal-bearing mechanisms. Other features include the tracking system made of light dependent resistance sensors, a direct current motor, a pulley, a belt, an Arduino controller, and a thermal energy storage tank. The lagging material was an expanded Polyethylene sheet. Experimental data were measured with thermocouples, a digital panel, a Uni-T digital anemometer (UT363), and a digital solar power meter (SM206-SOLAR). Matrix Experimental design was used to develop an experimental model for the system. The developed system was tested to investigate the effect of various heat collectors with and without coating on its performance. It was established from the response optimization that the intercept factor was improved by 32.2%. Similarly, the theoretical efficiency was improved by 8.19% while the experimental thermal efficiency was improved by 6.99%.

Keywords: Solar; Receiver; Elliptical; Optimization; Intercept-factor

1. Introduction

The history of solar elliptical vessel receiver goes back over 130 years. A steam engine powered by John Ericsson was the first to employ elliptical vessel receiver in 1880 [1]. Shumand and Boys implemented this concept for irrigation in the Nile River region in 1912 [2]. Elliptical vessel receiver's extensive range of applications is a magnet for researchers. Numerous researchers are enticed to explore the diverse applications of elliptical vessel receiver. The paramount application of elliptical vessel receiver lies in its ability to generate electricity, capable of reaching temperatures of up to 400^{o}C. [3]. In addition to its high-power capability, high efficiency, modularity, and versatility, elliptical vessel receiver is also durable against moisture and it has a long life span. Additionally, it has disadvantages, such as receiver deformation, moving parts, high upkeep costs of the tracking system, and large land areas [4, 5]. The integration of traditional gas-powered power plants and concentrated solar systems such as elliptical vessel receiver enhances the overall efficiency of the system, resulting in reduced costs for electricity generation. Additionally, this arrangement can serve as a reliable backup support. [6]. By 2010, the capacity of global CSP plants was approximately 1 GW. It is anticipated that this capacity will experience a growth of 7% and 25% by the years 2030 and 2050, respectively. [7]. Reddy and Kumar (2012) conducted a study on electric power generation utilizing oil and water for heat transfer. They performed a techno-economic feasibility assessment of a solar vessel power plant across 58 various sites in India. Their

* Corresponding author: Aka C. C

findings indicated that the most efficient setup for the collector field is 6 meters in size with a rim angle of 65° [8]. Solar power offers numerous benefits to humanity, and various scientists have dedicated their efforts to exploring its diverse applications. The majority of researchers are currently focusing their efforts on studying this particular category of elliptical vessel receiver [7, 8]. The elliptical vessel receiver represents a linear concentrated solar collector. The physical components of an elliptical vessel receiver include the storage unit, reflector, locking unit, absorber, tracking unit, and structure. The main focus areas of elliptical vessel receiver are reflectivity, intercept factor, mass flow rate, heat transfer fluid (HTF), and applications, which researchers are currently investigating. The reflector mirror concentrates direct solar energy onto the elliptical vessel receiver, while the tracking system assists the vessel in following the sun's direction. The receiver then converts the solar energy into thermal energy, which is transferred to the HTF, hence the quest for this design modification.

2. Materials and Method

The resources utilized in this research were obtained from Kenyeta Market Enugu, Onitsha Bridge Head Market, and Idumota Market Lagos, all of which are local sources. These materials were sourced based on categories of components element: support mechanism made of mild steel (MS) plates, bolts, and nuts, clamps, heat transfer fluid using water, reflector made of chrome tickers, aluminum foil tape, glass cover, bolts, and nuts. Besides were receivers made of copper pipe, aluminum pipe, galvanized iron (G.I.) pipes, chlorinated polyvinyl chloride (CPVC) ($^{3}/_{4}$) pipes, stainless steel pipes, and journal bearing mechanisms. Among other category components was a tracking system made of Light Dependent Resistance (LDR) sensors, a direct current (DC) motor, a pulley, a belt, and an Arduino controller. Besides was thermal storage made of high thermal energy storage capacity, commercial grade acetanilide, and expanded Polyethylene (EPE) sheet. The measuring devices were of thermocouple, digital panel, Uni-T digital anemometer (UT363), and digital solar power meter (SM206-SOLAR).

The design and construction of the elliptical vessel receiver were mainly driven by its intended applications, leading to the incorporation of various additional components in the system. Along with the support mechanism, receiver element, HTF, tracking system, concentrating reflector, and thermal storage device are all part of the elliptical vessel receiver system.

2.1. Design Modification of Elliptical Vessel Solar Receiver

The literature review provided the basis for determining the design considerations of the elliptical vessel receiver (EVR). The key factors for the geometric configuration of an elliptical vessel receiver included the length of the vessel, rim angle, aperture width, and focal length. Designing a vessel receiver posed a substantial difficulty. However, it was crucial to also take into account other influential parameters such as average wind speed, heat transfer fluid (HTF), application, number of loops, and storage device, as they all contributed to the overall conversion efficiency of the system and its economic benefits.

Taking all these parameters into consideration, a new elliptical vessel receiver design was developed, which facilitated easy accumulation and transportation. Specific provisions were made to accommodate different reflector sheets, different absorber pipes, and different HTFs. Furthermore, the design allowed for adjustments in the vessel's geometric dimensions. Furthermore, it had features for attaching a storage device and an automated tracking system. This design effectively addressed the issue of flexible joints used in conventional elliptical vessel receiver designs, thereby eliminating the problem of leakage commonly encountered in such systems.

2.1.1. Geometrical parameters

The elliptical vessel receiver is characterized by its geometric properties. The primary properties include the length of the vessel (l), the width of the aperture (a), the angle of the rim (ψ), and the focal length (f) as depicted in Figure 1.

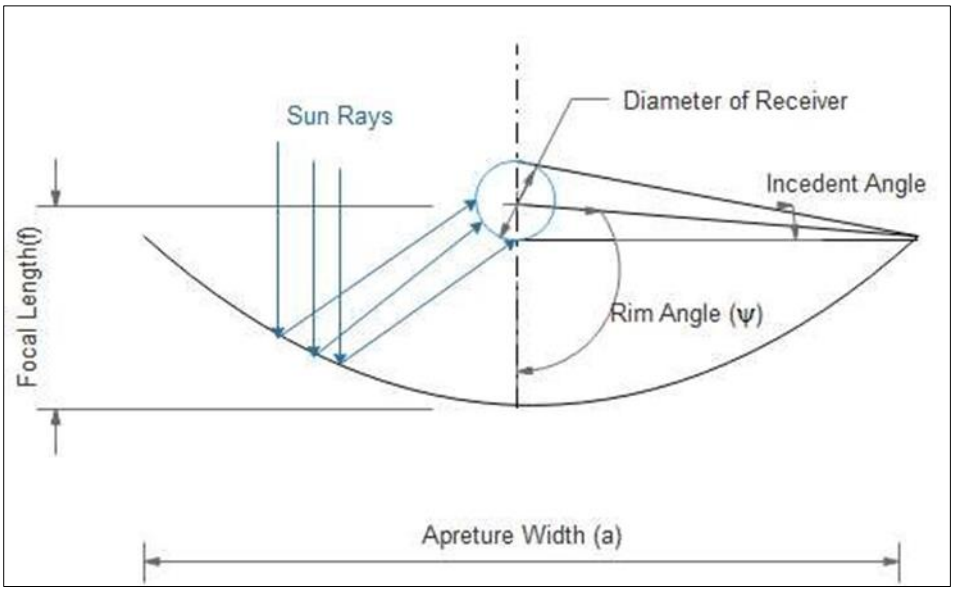

Figure 1 Geometry of Vessel

The elliptical shape suitable analytical description is determined by [9].

$$Y = \sqrt{4fX} \quad \ldots\ldots\ldots\ldots\ldots\ldots\ldots \quad (1)$$

Where X and Y are the x and y coordinates and the distance (f) represents the measurement between the vertex of the parabola and the focal point, which was utilized for the calculation and modeling of the parabola's shape.

Three critical criteria were considered to calculate the cross-sectional form along with the dimensions of an elliptical vessel: rim angle, aperture width, and focal length. The third parameter might be computed by determining the correlation between both of these variables. More specifically, the rim angle was expressed as the function of the focal length and the aperture width. [10]. As in Equation (2)

Thus.

$$\frac{a}{f} = -\frac{4}{tan\ \psi} + \sqrt{\frac{16}{tan\psi^2} + 16} \quad \ldots\ldots\ldots\ldots.. (2)$$

The aperture area (A_a) was determined by the product of length of Vessel (l) and aperture width (a) [10]. See Equation (3)

$$A_a = a\ x\ l \quad \ldots\ldots\ldots\ldots\ldots\ldots\ldots (3)$$

The surface area of an ELLIPTICAL Vessel is essential to ascertain the material necessary for the Vessel. The area is premeditated as follows in as in Equation (4) noted by [10].

$$A_s = \left(\frac{a}{2}\sqrt{1 + \frac{a^2}{16f^2} + 2f \times ln}\left(\frac{a}{4f} + \sqrt{1 + \frac{a^2}{16f^2}}\right)\right) \times l \quad \ldots\ldots\ldots\ldots\ldots. (4)$$

Where f is the focal length of the vessel, a is aperture width and ln is the natural logarithm

One of the crucial receiver characteristics is the concentration ratio (C). The potential working temperatures of the elliptical vessel receiving system depend on it. A ratio of the aperture area (A_a) to the receiver area (A_r) is what is termed the general concentration ratio (C). [1, 3, 4]. As in Equation (5)

$$C = \frac{A_a}{A_r} \ldots\ldots\ldots\ldots\ldots\ldots (5)$$

In this particular design, the length of the vessel was altered by adjusting the length of the angular bar. This angular bar was securely fastened to the crossed pipe, which was in turn connected to the bearing. In the present design, the vessel's length measured 98 cm (980mm). The aperture width, denoted as (a), represents the width of the vessel and it was set at 67 cm (670mm) and remained fixed on the bearing.

The rim angle (ψ) is crucial in determining the relationship between the axis of the receiver pipe and the line connecting the focal point and the mirror rim. Choosing the appropriate rim angle is of utmost importance. A vessel with a low rim angle will result in a non-dimensional aperture area and a concentrator with less curvature and a longer focal length [11]. A robust and extended receiver support is essential for the concentrator to ensure that the center of gravity is shifted away from the concentrator's axis. This is necessary to minimize bending and the need for higher torque during tracking. Additionally, concentrating solar energy on a smaller area of the receiver's surface leads to a higher local concentration ratio and a larger thermal gradient. While a higher rim angle offers the advantage of a smaller focal distance, it also requires a greater curvature of the concentrator. In this particular design, a rim angle of 99 degrees is chosen.

Focus length (f) is a measurement of how far the focal point is from the vertex of the parabola. Parabolas are entirely defined by this factor. In this project, 26.9 cm is taken. The vessel is constructed from a 25.4 mm mild steel angle bar and has a glass top to keep out dust and increase the experimental thermal efficiency. The geometrical features of the developed Vessel are displayed in Figure 2.

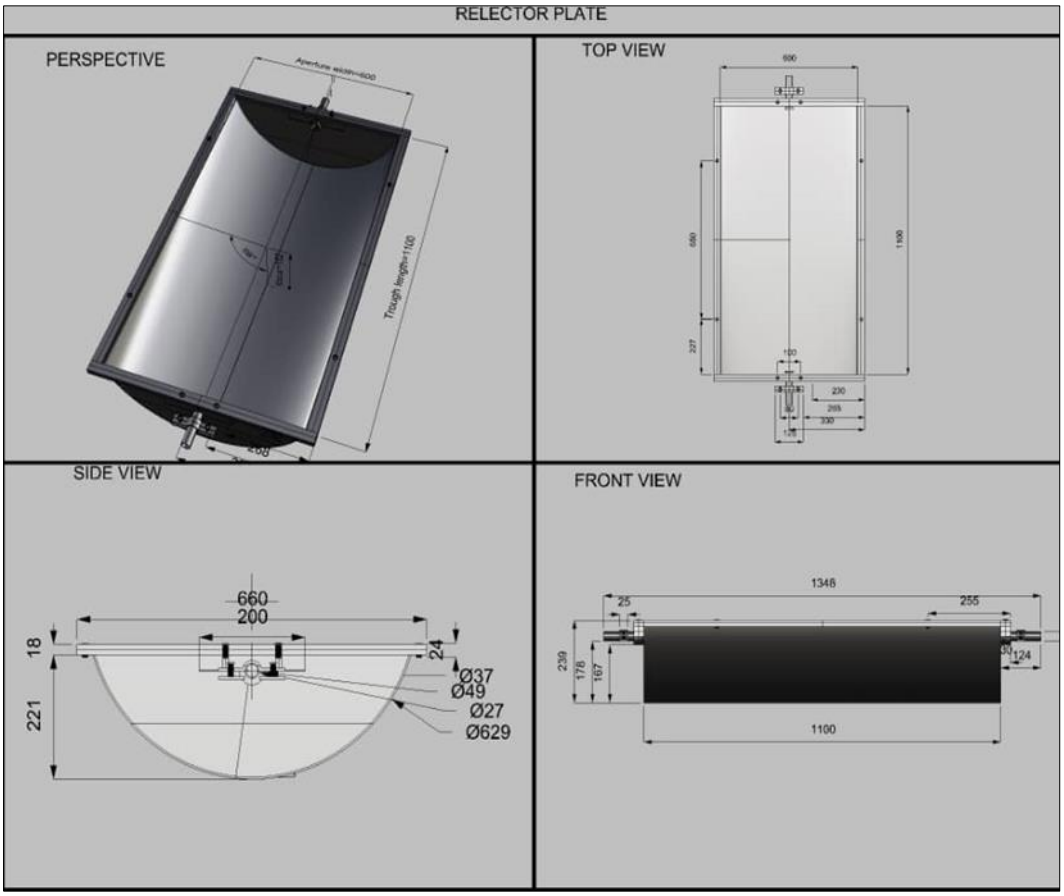

Figure 2 Geometrical Descriptions of Vessel

2.1.2. Stands Development

The stand possesses a cradle-shaped structure and offers enhanced stability while the vessel is oscillating. To ensure stability, a vertical angle bar is welded between the two legs of the stand. Additionally, two stands are linked together

with a horizontal angle bar to resist vibration and deflection. The top of the stand features a clamping arrangement that securely holds the Vessel. This clamping arrangement is illustrated in Figure 3.

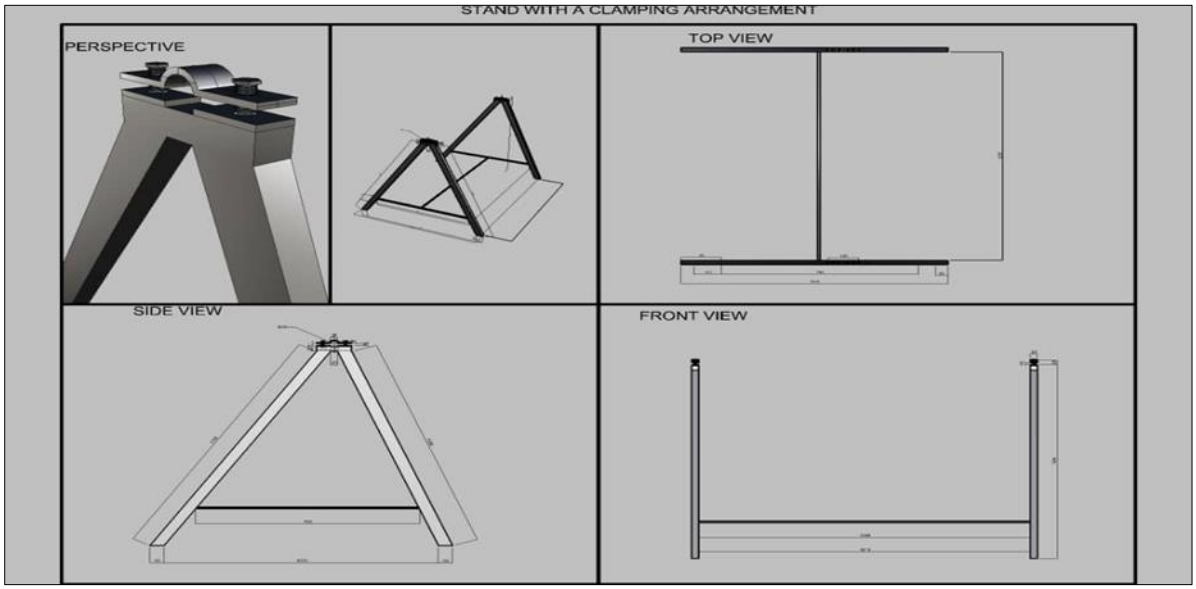

Figure 3 Stand with a clamping arrangement

2.1.3. Receiver Pipe Joints Development

The design includes a receiver pipe with a diameter of 25.4 mm originally, there was a flange on the vessel side that allowed for the attachment of various receiver pipes to the system. However, this flange has been replaced by a CPVC (19.05mm) union joint, which is inserted in a bearing to enable smooth rotation of the vessel. The union joint is securely fixed on the stand's clamp. Initially, a stainless steel (SS) pipe with a diameter of 25.4 mm was chosen, but it was replaced by a 19.05mm CPVC pipe as the material for the support pipe. This unique arrangement has effectively resolved issues such as bending, flexible joints, and leakage in the receiver pipe. Moreover, thanks to the union joint, it is now convenient to replace different receivers for efficiency testing. This can be seen in Figure 4.

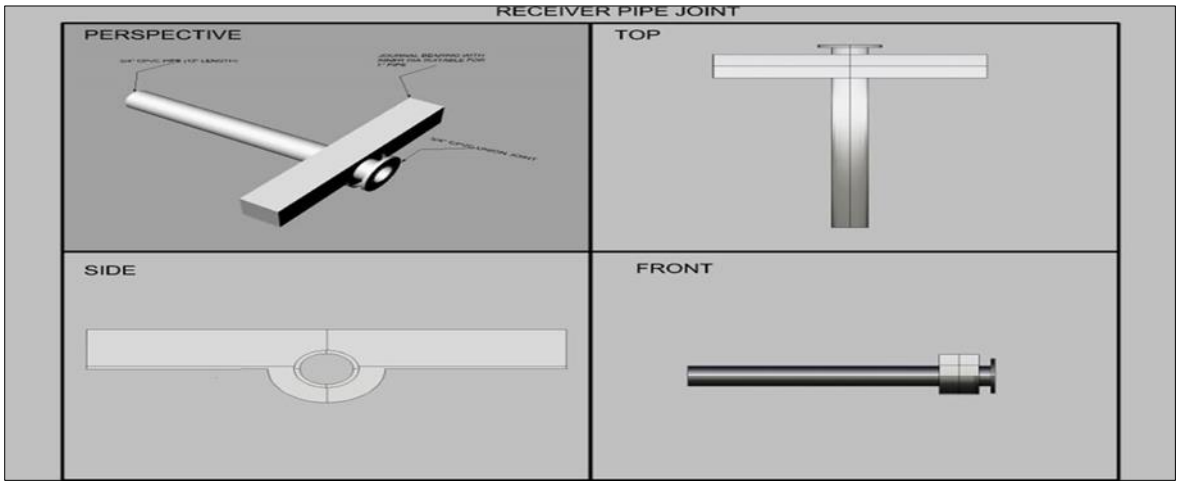

Figure 4 Receiver Pipe Joint

2.1.4. Width Angular Bar Development

A vertical angular bar of 67 cm (670mm) was connected with journal bearing. It represents the vessel's aperture width (a). The structure is made of a 25.4mm rectangular bar of mild steel. There are holes drilled at each end of the vessel to connect the angular bars. This is illustrated in Figure 5.

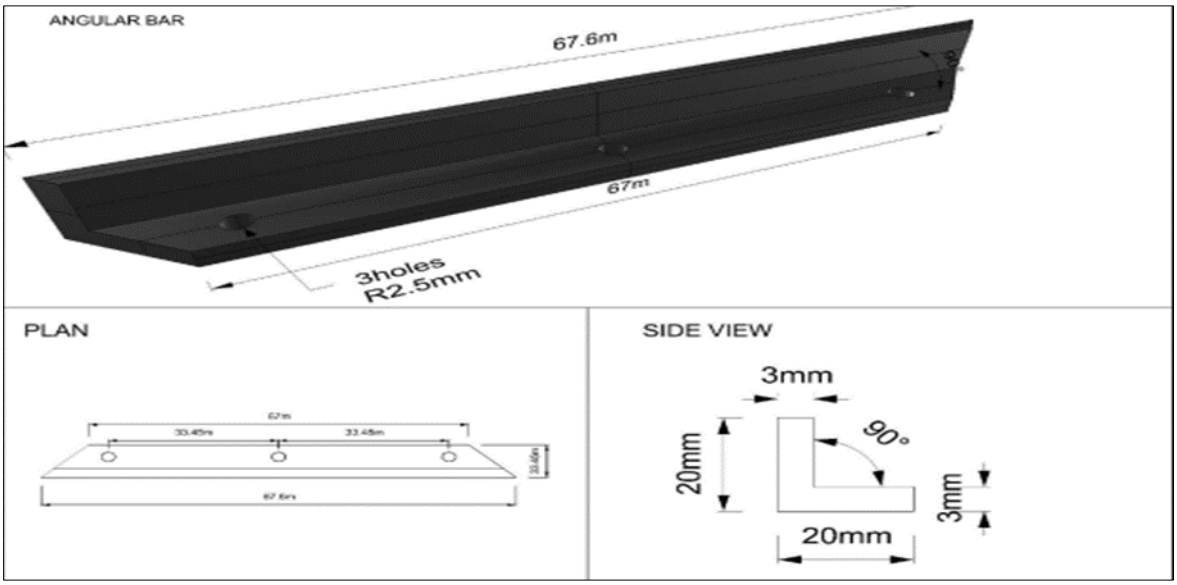

Figure 5 Width Angular Bar

2.1.5. Length Angular Bar Development

A 98 cm mild steel angular bar is utilized in this case to represent the length of the vessel. The ends of the bar are drilled and threaded, allowing it to be attached to the angular bar using a journal bearing. By adjusting the length of the bar, we have the ability to alter the length of the vessel. This information is depicted in Figure 6.

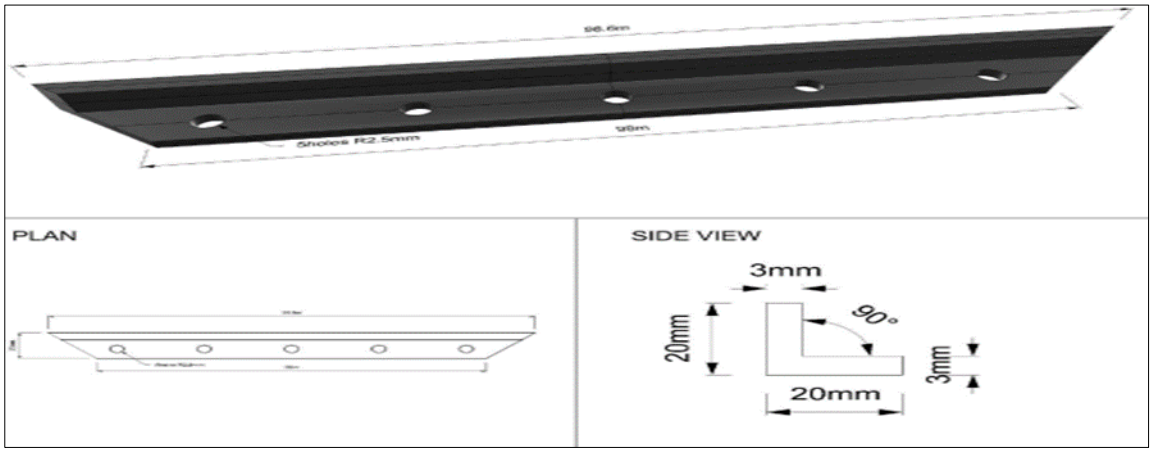

Figure 6 Length Angular Bar

2.1.6. Reflector Holding Vessel Development

The combination of two angular width bars and two angular length bars resulted in the formation of a rectangular top for the Vessel. The elliptical shape of the reflector is made by this vessel like body made with mild steel which serve as the reflector holder. These vessel like body are bolted with length angle bar of the Vessel as well as the angular width bar to their four edges. This holding body embodies the reflective sheet of various reflective materials and as well help to increase the radiation heat flux by preventing radiation lost from the reflector and absorber surfaces. By this arrangement, one can easily change reflectors and it will still retain same focal length of the parabola. The vessel displayed in Figure 3.7.

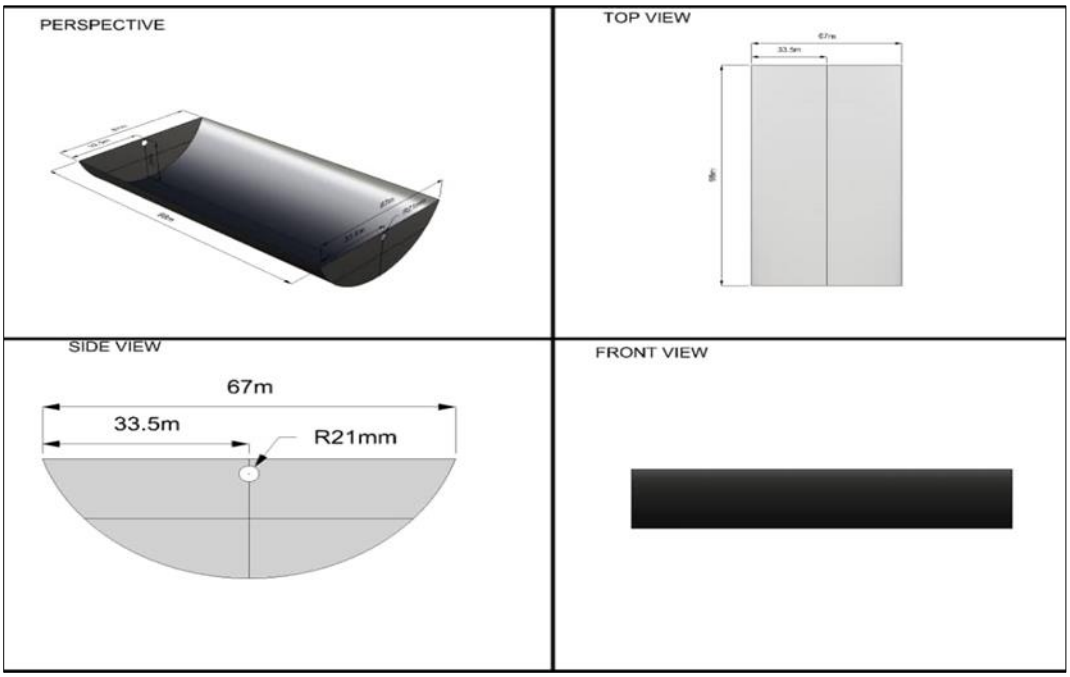

Figure 7 Reflector Holding Vessel

2.1.7. Automatic Tracking System

Special design considerations are present in the Novel elliptical vessel receiver. To limit movement and fix the vessel for tracking, locks are used. The receiver pipe is fastened to the vessel body by bearing mechanisms. These configurations allow the vessel to spin with minimal effort. The tracking mechanism does not need large motors or gearboxes. For a revolving vessel, a basic DC 12 V 10 rpm geared motor is sufficient. A DC motor is used to rotate a pulley that is attached to a rope. The sun is tracked using LDR sensors. A microcontroller called an Arduino controller is utilized for automated tracking. Figure 8, display the automated tracking system.

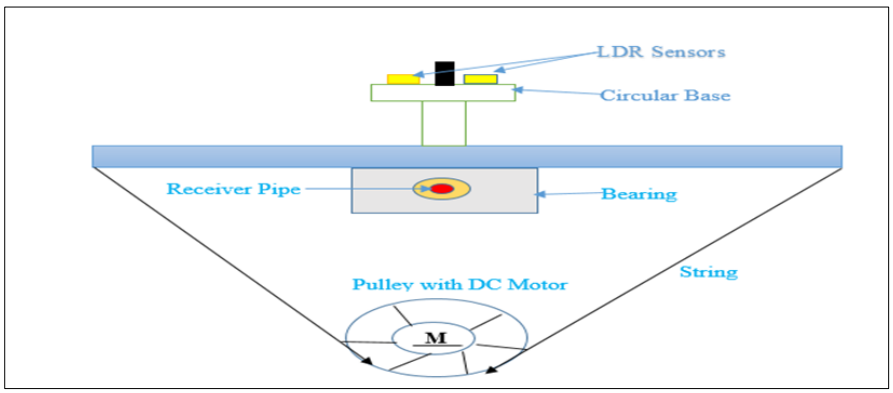

Figure 8 Automatic Tracking Arrangements

2.1.8. Locking System

The designed elliptical vessel receiver has a locking mechanism linked to it that holds the vessel elements in a position that is protected from strong winds and storm damage. The current invention stipulates that after the motive-drive system, which is in sync with the tracking unit and the LDR sensor, moves the vessel of the receiver to that position of high solar intensity, a bolt mechanism locks the vessel into that protected position. The locking mechanism is disengaged when is starting to track and is activated when it stops tracking. A locking bar that is fastened straight to the side of the vessel is where the locking mechanism latches and locks.

2.1.9. Glass Cover Attachment

The glass cover attachment serves to shield the Vessel from dust and wind. The upper frame of the Vessel is constructed using square pipes in a rectangular configuration. The glass cover is crafted from aluminum sections and connected to the upper frame through hinges. Thanks to these hinge placements, the receiver and reflector can be easily replaced. The sides of the Vessel are enclosed by MS plates. With the glass cover in place, the infrared radiation in the form of reflected energy is contained within the Vessel. The first construction stage of vessel model with glass cover in design stage is shown in Plate 1 and 2.

Plate 1

Plate 2

Plate 1 and 2 Construction Stage of Vessel with Glass Cover

2.1.10. Assembly of the Elliptical Vessel Receiver (elliptical vessel receiver)

Utilizing Computer Aided Design (CAD), the model was successfully fabricated. This prototype is known for its exceptional flexibility, making it possible to transport in a taxi. The assembly of the fabricated model can be seen in Figure 9, while Table 1 provides the final dimensional values of the system.

Table 1 Final Dimensional values

Description	Values
Vessel length	0.98 m
Vessel Width	0.67 m
Concentration ratio	11.87≈12
Focal distance	0.269 m
Rim angle	990

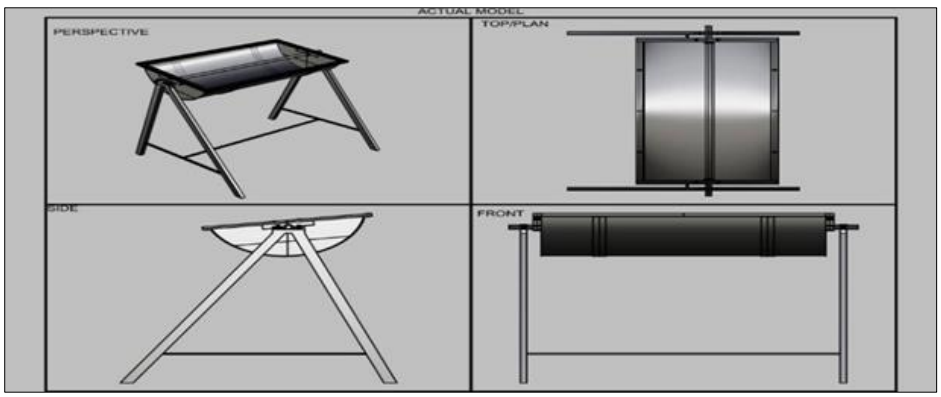

Figure 9 Actual Model

3. Results and Discussion

The complete factorial multi-functional multi-level design of experiment (DOE) of Table 2 was applied. The experiment was performed using the 'M x N' matrix design approach as stated in Table 2 where M equals 4 and donates the number of samples, and N donates the degree of freedom which equals three plus one (3+1). For the design matrix, 0 means no combination or pair while 1 donates a pair of samples and degree of freedom. From Table four samples were tested uncoated and they were also tested with three coating elements making a total of 16 run levels. However, 48 efficiencies were calculated. Table 2 denotes the average values of input parameters which were measured on experimentation day.

Table 2 Result of Experiment Setup Design

Sr. No.	Samples	Intercept Factor (γ)	Receiver (α)	Degree of Freedom Combination (N)		
				Polyurethane	Turmeric	Shred Tyre
1	Copper	0.341	0.3	0	0	0
2	Copper	0.341	0.98	0	0	1
3	Copper	0.341	0.67	0	1	0
4	Copper	0.341	0.56	1	0	0
5	Aluminium	0.341	0.16	0	0	0
6	Aluminium	0.341	0.91	0	0	1
7	Aluminium	0.341	0.58	0	1	0
8	Aluminium	0.341	0.38	1	0	0
9	Galvanized Iron	0.341	0.44	0	0	0
10	Galvanized Iron	0.341	0.84	0	0	1
11	Galvanized Iron	0.341	0.62	0	1	0
12	Galvanized Iron	0.341	0.44	1	0	0
13	Stainless Steel	0.341	0.37	0	0	0
14	Stainless Steel	0.341	0.72	0	0	1
15	Stainless Steel	0.341	0.51	0	1	0
16	Stainless Steel	0.341	0.32	1	0	0

Table 3 Result of Measured Input Parameters

Sr. No.	Testing Parameters		Measured Data					
	Intercept Factor (γ)	Receiver (α)	T_i (°C)	T_o (°C)	I_{rb} (W/m^2)	V (m/s)	T_r (°C)	T_a (°C)
1	0.341	0.3	35.13	45.35	829.33	1.37	37.30	29.80
2	0.341	0.98	32.00	46.75	606.73	1.36	30.13	29.78
3	0.341	0.67	38.03	52.68	829.47	1.77	44.87	39.68
4	0.341	0.56	34.02	46.58	797.73	1.53	42.07	35.07
5	0.341	0.16	34.05	38.76	848.07	0.97	36.80	29.80
6	0.341	0.91	33.70	52.06	802.53	1.71	57.37	32.02
7	0.341	0.58	36.24	49.64	836.33	1.69	44.81	34.69
8	0.341	0.38	34.80	41.95	811.53	2.04	50.29	32.17

9	0.341	0.44	34.92	45.93	893.13	1.62	53.37	31.97
10	0.341	0.84	35.04	51.68	717.53	2.34	51.24	30.57
11	0.341	0.62	34.67	46.59	796.53	1.56	36.26	39.63
12	0.341	0.44	31.82	40.36	795.40	1.47	48.23	34.77
13	0.341	0.37	34.23	42.48	811.53	1.37	56.01	30.62
14	0.341	0.72	36.13	52.96	774.47	1.41	46.85	34.52
15	0.341	0.51	33.93	43.73	721.47	2.19	51.07	30.57
16	0.341	0.32	30.45	36.90	790.93	1.40	38.46	35.15

Various efficiencies were calculated using equations from chapter three and measured input data. In Table 4, the average values for all efficiencies are shown.

Table 4 Calculated Data for Efficiencies

Sr. No.	**Testing Parameters**		**Calculated Efficiency**		
	Intercept Factor (γ)	**Receiver (α)**	**η_{thexp} (%)**	**$\eta_{opt\ theo}$ (%)**	**η_{theo} (%)**
1	0.341	0.3	9.82	7.10	7.09
2	0.341	0.98	19.37	23.20	23.19
3	0.341	0.67	14.08	15.86	15.85
4	0.341	0.56	12.55	13.25	13.24
5	0.341	0.16	4.42	3.79	3.78
6	0.341	0.91	18.26	21.54	21.50
7	0.341	0.58	12.77	14.67	14.66
8	0.341	0.38	7.03	8.99	8.96
9	0.341	0.44	9.83	10.41	10.38
10	0.341	0.84	18.50	19.88	19.84
11	0.341	0.62	11.94	13.73	13.73
12	0.341	0.68	8.53	10.41	10.39
13	0.341	0.37	8.10	8.76	8.72
14	0.341	0.72	17.34	17.04	17.02
15	0.341	0.51	10.84	12.07	12.03
16	0.341	0.32	6.50	7.57	7.57

It can be seen from the recorded and calculated data in Table 3 that experimental efficiency rises as the receiver absorption coefficient increases since the intercept factor is constant. Figure 2 shows a strong correlation between efficiencies and variables. Efficiency was not much affected but the changes in the emissivity of any of the combinations, demonstrated that only the absorptivity and intercept factor are important contributors and therefore validating the experimental approach.

The ANOVA parameter tables, including method, factor information, analysis of variance, model summary, and means, were presented in Appendix D. The general factorial regression analysis utilizing Tables 5 and 6 for a one-way ANOVA indicated that the p-value for both tables is below the significance level of 0.05. Consequently, both factors were considered significant in the analysis.

Table 5 One–Way ANOVA table for η_{thexp} Using Significant Value of 0.05

General Factorial Regression for η_{thexp} Against Intercept Factor (y), Receiver (α)					
Source	DF	Adj SS	Adj MS	F-Value	P-Value
Receiver	14	329.935	23.5668	27.89	0.015
Error	1	0.845	0.8450		
Total	15	330.780			
S=0.919239	R-sq= 99.74%		R-sq(adj)= 96.17%		

Table 6 One-Way ANNOVA table for η_{theo} Using Significant Value of 0.05

General Factorial Regression for η_{theo} Against Intercept Factor (y), Receiver (α)					
Source	DF	Adj SS	Adj MS	F-Value	P- Value
Receiver	14	449.179	32.0842	641684.71	0.001
Error	1	0.000	0.0001		
Total	15	449.179			
S= 0.0070711	R-sq.= 97.93%		R-sq. (Adj)=96.08%		

Figures 10 and 11 display the main effect plot, indicating that a higher absorptivity value factor leads to increased experimental efficiency for η_{thexp}. The receiver pair with an absorption coefficient of 0.98 has the highest efficiency recorded. The main effect plot demonstrates that a higher absorptivity coefficient correlates with greater efficiency, ultimately concluding that the receiver with a coating value of 0.98 is the most efficient. In this context, the receiver emerges as the most crucial element, establishing it as the dominant factor. The R-squared values are 99.74% and 97.93% for η_{theo} and η_{thexp} respectively.

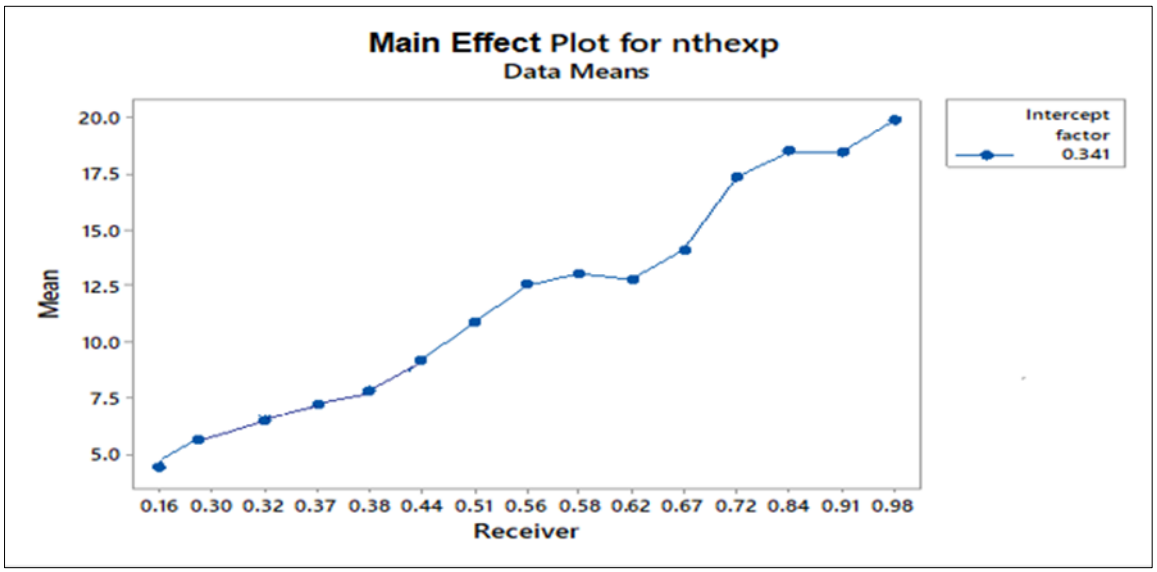

Figure 10 Main Effect Plot for η_{thexp}

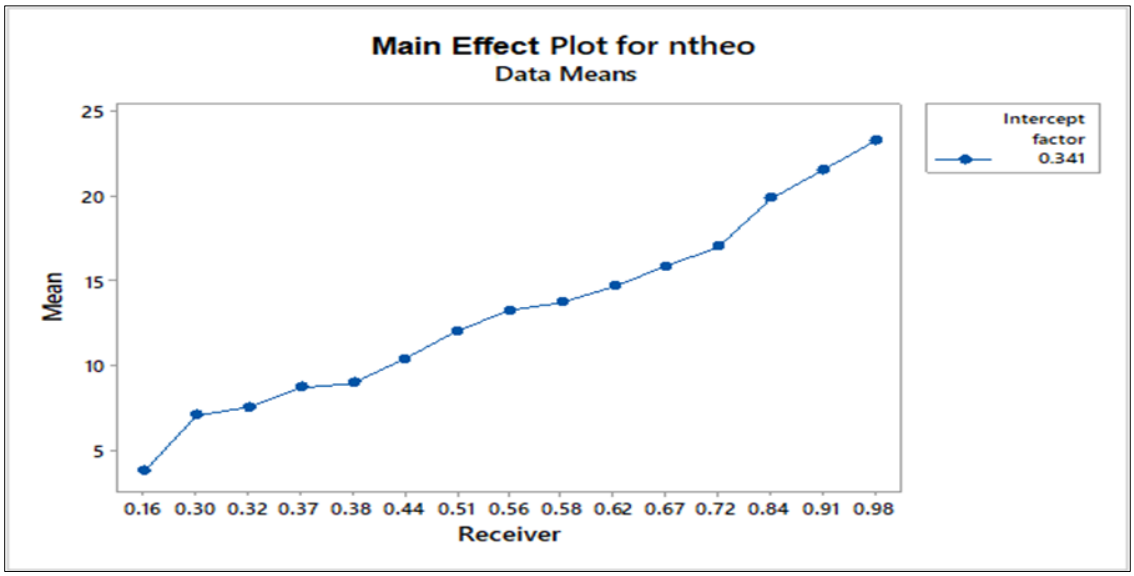

Figure 11 Main Effect Plot for $\boldsymbol{\eta_{theo}}$

Analysis of the main effect plots presented in Figures 10 and 11 demonstrates that the thermal experimental efficiency exhibits a positive correlation with the absorptivity of the receivers. The graphs vividly depict the relationship between efficiencies and factors. Notably, as the level of the factors is elevated in both cases, efficiency also increases, signifying the importance of these factors. Consequently, the experimental process is confirmed to be valid. The interval plot of the absorptivity against efficiencies is depicted in Figure 12. Since all three efficiencies $\eta_{thexp,}\, \eta_{optheo}$ *and* η_{theo} have overlapped with all the absorption coefficients and since higher absorptivity values gained higher efficiencies. The data demonstrates a strong correlation between the experimental efficiency results and both the optical theoretical efficiency and the theoretical efficiency. As a result, the receiver value of 0.98 stands out as the most impactful, surpassing other receiver values in terms of all efficiencies.

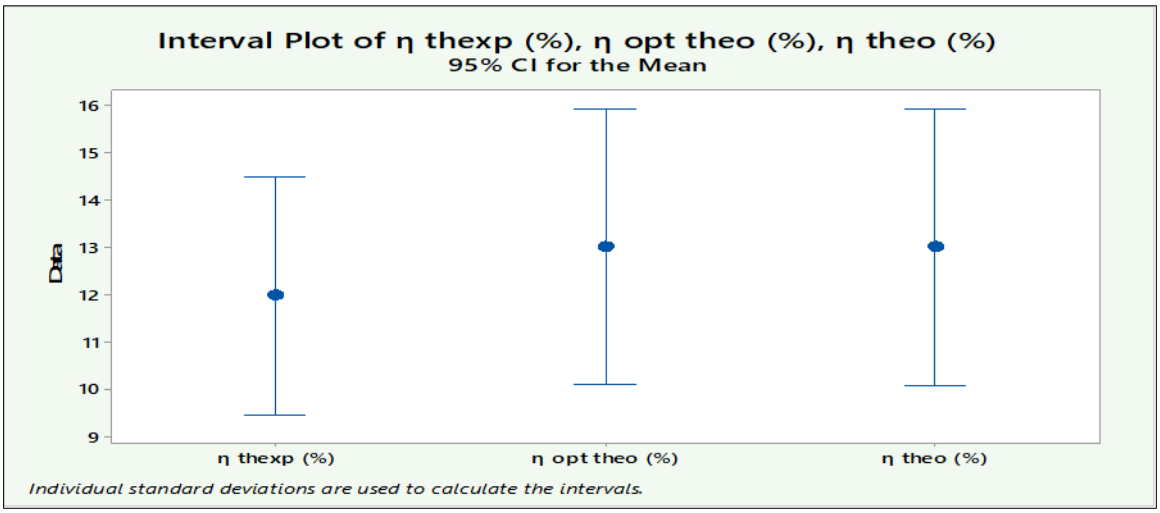

Figure 12 Interval Plot of Receiver (α) against Efficiencies

Table 7 Result of Response Optimization for η_{theo}, η_{exp}

	Response Optimization for η_{theo}, η_{thexp}				
	Intercept Factor	**Receiver (α)**	η_{theo} **Fit**	η_{thexp} **Fit**	**Composite Desirability**
Old Design [12]	0.231	0.98	15.28	12.38	0.98
Improved Design	0.341	0.98	23.19	19.37	0.98
% Response Optimization	32.2	0	8.19	6.99	0

With the presented data, response optimization was done; a better context was chosen to achieve greater efficiency. The combination of an intercept factor of 0.341 and a receiver absorptivity coefficient value of 0.98 is the best-fitted pair in Table 4.6 as a solution. The highest efficiency is delivered by the aluminum foil reflector and copper receiver with shred tyre carbon coating, giving η_{thexp} = 19.37% and η_{theo} = 23.19%. The efficiency results are equitably consistent with [13, 14, 15].

The given equations in the previous chapter were used to compute the experimental, optical, and theoretical efficiencies. Experimentally, determining optical efficiency is exceedingly challenging. It is challenging to match the correlation between practical and theoretical efficiency since optical efficiency is frequently evaluated using numerical methods. An analysis was carried out to compute the efficiencies based on experimental data, indicating that the discrepancies between the experimental and theoretical efficiency values fall within a 5% range. In contrast, the optical and theoretical efficiency values showed no significant deviations. It was established from the response optimization that the intercept factor was improved by 32.2%. Similarly, the theoretical efficiency was improved by 8.19% while the experimental thermal efficiency was improved by 6.99%.

4. Conclusion

A portal and multipurpose elliptical vessel receiver have been designed, developed, and tested with local contents, incorporating a synchronized tracking and locking system, and greater efficiency was achieved. This increased overall efficiency can drive advancements in sustainable energy extraction and the mitigation of greenhouse gas emissions. However the effect of glass cover on sun irradiation has to be studied afterwards.

Compliance with ethical standards

Disclosure of conflict of interest

The authors declare that there is no conflicts of interest

Author contribution

All authors contributed equally to this work.

Data availability statement

The data that supports the findings of this study are available on request from corresponding author

References

[1] A. J. Abdulhamed, N. M. Adam, Ab-Kadir, M. Z. A., A. A. Hairuddin and M. Zainal, "Review of solar parabolictrough collector geometrical and thermal analyses, performance , and applications.," Renewable and Sustainable Energy Reviews, vol. 91, p. 822–831, March 2018.

[2] C. Haddock and J. S. C. ,. Mckee, "Solar Energy Collection, Concentration, and Thermal Conversion — A Review.," Energy sources, vol. 13, no. 4, p. 461–482, 2007.

[3] V. Jebasingh and G. J. Herbert, "A review of solar parabolic trough collector," Renewable and Sustainable Energy Reviews, vol. 54, p. 1085–1091, 2016.

[4] A. Hafez, A. Attia, H. Eltwab, A. ElKousy, A. Afifi, A. AbdElhamid, A. AbdElqader, S. E. Fateen, K. El-Metwally, A. Soliman and I. Ismail, "Design analysis of solar parabolic trough thermal collectors.," Renewable and Sustainable Energy Reviews, vol. 82, p. 1215–1260, 2018.

[5] K. Kaygusuz, "Environmental Impacts of the Solar Energy Systems," Energy Sources, Part A: Recovery, Utilization, and Environmental Effects, p. 1376–1386., 2009.

[6] G. D. Yogi, "Solar Thermal Power Technology: Present Status and Ideas for the Future," Energy Sources, vol. 20, no. 2, p. 137–145, 1998.

[7] A. Ummadisingu and M. Soni, "Concentrating solar power – Technology, potential and policy in India," Renewable and Sustainable Energy Reviews, vol. 15, no. 9, p. 5169–5175, 2011.

[8] K. Reddy and K. R. Kumar, "Solar collector field design and viability analysis of stand-alone parabolic trough power plants for Indian conditions," Energy for Sustainable Development, vol. 16, no. 4, p. 456–470., 2012.

[9] J. A. Duffie, W. A. Beckman, W. M. Worek, J. A. Duffie, A. Beckman W. and W. M. Worek, Solar Engineering of Thermal Processes, Fifth Edition ed., Hoboken, New Jersey: John Wiley & Sons, Inc., 2020.

[10] M. Günther, M. Joemann, S. Csambor, M. Günther, M. Joemann and S. Csambor, Parabolic Receiver Technology, no. chapter5, 2014.

[11] G. Kumaresan, R. Sridhar, R. & Velraj, G. Kumaresan, R. Sridhar and R. & Velraj, "Performance studies of a solar parabolic trough collector with a thermal energy storage system," Energy, vol. 47, no. 1, p. 395–402. , 2012.

[12] B. H. Upadhyay, A. J. Patel, P. V. Ramana, B. H. Upadhyay, A. J. Patel and P. V. Ramana, "Parabolic Trough Collector, a Novel Design for Domestic Water Heating Application," IJRASET, vol. 5, no. X, p. 497–503, 2020.

[13] A. Bharti, A. K. Mishra, B. Paul, A. Bharti, A. K. Mishra and B. Paul, "Thermal performance analysis of small-sized solar parabolic trough collector using secondary reflectors," International Journal of Sustainable Energy, vol. 38, no. 10, p. 1002–1022, 2019.

[14] D. Kumar and S. Kumar, "Thermal performance of the solar parabolic trough collector at different flow rates: an experimental study," International Journal of Ambient Energy, vol. 39, no. 1, p. 93–102, 2018.

[15] B. H. Upadhyay, A. J. Patel, P. V. Ramana, B. H. Upadhyay, A. J. Patel and P. V. & Ramana, "Comparative study of parabolic trough collector for low-temperature water heating," Energy Sources, Part A: Recovery, Utilization, and Environmental Effects, p. 1–17, 2019.